Measurements of electron beam distribution in phase space

Kiminori Goto
Department of Physics,
Hiroshima University,
1-3-1 Kagamiyama,
Higashi-Hiroshima, 739, Japan

Abstract

A possible use of the parametric x rays(PXR) as a beam diagnostic tool is discussed. In the proposed method, the spatial and angular distributions of the beam are found out, at the same time and directly, by measuring the PXR from a tiny crystal exposed to a various part of the beam. We made a test measurement of the electron beam from the Tokyo Synchrotron using a silicon crystal($2\times2mm^2$). It has been found that space-angular correlation can be measured by the new method based on the PXR and that the theoretical formula describing of PXR has to be improved in order to obtain the more accuracy information of the electron divergence.

Contents

1 Introduction

Accelerators have come to play an important role not only in science but also in various fields. As the more precise measurement is required, the more important beam informations(or conditions) of an accelerator have become. The information have been measured by various methods[6, 8]. Distributions of particles in the beam are represented by the shape in the density distribution of points in the phase space;(x, x') and (y, y'), where x and y are positions perpendicular to the beam direction, while x' and y' are angular divergences, respectively, in horizontal and vertical planes. There is a correlation between x and x'(or y and y'). Twiss parameters and Emittance(;see next section) are used as indices to represent a beam condition. For the case of a beam line, however, there have been no way to obtain beam parameters by a measurement of spatial and angular beam distributions at the same time. Twiss parameters and emittance are usually determined by calculating the data of spatial distribution for various operating conditions of the beam line, based on the orbit theory[7]. It is, therefore, desirable to develop a direct method to measure the beam parameters.

When a relativistic electron beam incident on a crystal, the parametric x rays(PXR) are emitted satisfying almost the same kinematical relation as those in the x-ray diffraction. The direction, where PXR is radiated into a well defined cone around $2\theta_B$(,where θ_B is called Bragg angle), is sensitive to the incidental angle of an electron so that the distribution of the electron angular-divergence could be measured directly. Since the intensity of PXR is proportional to the incident beam intensity, the spatial distribution of the beam is found out by measuring the PXR from a tiny crystal exposed to a various part of the beam. There is, therefore, a good possibility that the spatial and angular distributions of the beam are obtained at the same time.

This work aims at estimating whether PXR can be a beam diagnostic tool by measuring the correlation between the position(x) and the mean value of angular divergence(x') in the horizontal plane, using a tiny silicon crystal(area:2×2mm^2,thickness:0.5mm). In order to check the adequacy of the result, the beam parameters were also measured by the conventional method[6].

2 Theory

2.1 Beam Transport

Beam Ellipse Consider a large number of particles, and consider their distribution in the phase space of (x,x') at some point along the beam line or a circular ring. Assume the particle distribution at that point in the (x,x') space is a generalized Gaussian distribution. Take a contour(for instance, 1-σ) in the distribution. It will be represented by an ellipse in the (x,x') plane(Fig.1), like

$$\gamma x^2 + 2\alpha x x' + \beta x'^2 = \varepsilon \tag{1}$$

,where ε is the emittance and α, β and γ are parameters called as Twiss parameters. Twiss parameters follow the equation as,

$$\beta\gamma - \alpha^2 = 1 \ . \tag{2}$$

A tilt angle of the ellipse defined in Figure.1 is written as

$$\chi = \frac{1}{2}\tan^{-1}\frac{2\alpha}{\gamma - \beta} \ . \tag{3}$$

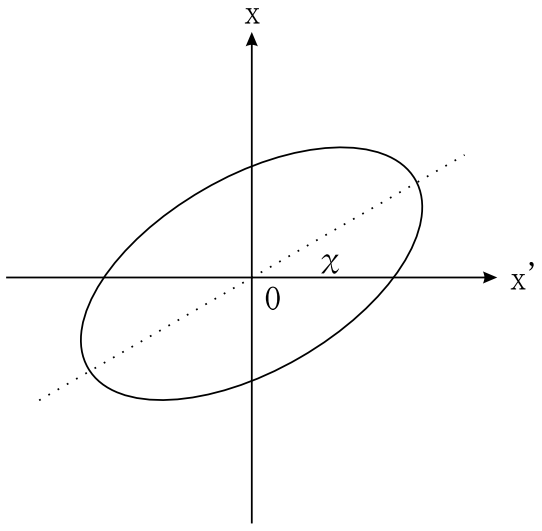

Figure 1: Beam ellipse in phase space.

Transfer of Beam Matrix

Twiss parameters are transported from position 1 to position 2 in a beam line or a ring, with keeping $\varepsilon = constant$. Define the matrix(called as a σ-matrix) as

$$\boldsymbol{\sigma} \equiv \varepsilon \begin{pmatrix} \beta & -\alpha \\ -\alpha & \gamma \end{pmatrix} , \tag{4}$$

and then the σ-matrix at position 2 is written as

$$\boldsymbol{\sigma}_2 = \boldsymbol{R}\boldsymbol{\sigma}_1\boldsymbol{R}^T \tag{5}$$

,where $\boldsymbol{R}$ is a transfer-matrix(appendix.A) between positions 1 and 2. And this equation is rewritten as

$$\begin{pmatrix} \beta \\ \alpha \\ \gamma \end{pmatrix}_2 = \begin{pmatrix} R_{11}^2 & -2R_{11}R_{12} & R_{12}^2 \\ -R_{21}R_{11} & 1+2R_{12}R_{21} & -R_{12}R_{22} \\ R_{21}^2 & -2R_{22}R_{21} & R_{22}^2 \end{pmatrix} \begin{pmatrix} \beta \\ \alpha \\ \gamma \end{pmatrix}_1 . \tag{6}$$

2.2 Parametric X Ray (PXR)

Coherent x rays, called PXR, are emitted satisfying almost the same kinematical relation as those in the x-ray diffraction when a relativistic electron passes through periodic medium. This phenomenon was first predicted by Ter-Mikaelian[1] and since then many theoretical and experimental works were performed.

2.2.1 Kinematics of PXR

Write 4-momenta of initial electron, final electron and PXR as (E_e, $\mathbf{p}$), (E_e', p') and (ω, $\mathbf{k}$), respectively, and then the energy and momentum conservation law leads to

$$E_e = E_e' + \omega , \tag{7}$$

$$\mathbf{p} = \mathbf{p}' + \mathbf{h} + \mathbf{k} , \tag{8}$$

where $\mathbf{h}$ is a reciprocal lattice vector. Fig.2 shows the diagram of kinematics for PXR.

Assume that the incident electron has high energy($E_e \gg$ electron mass m_e, ω), and then the energy of emitted photon is

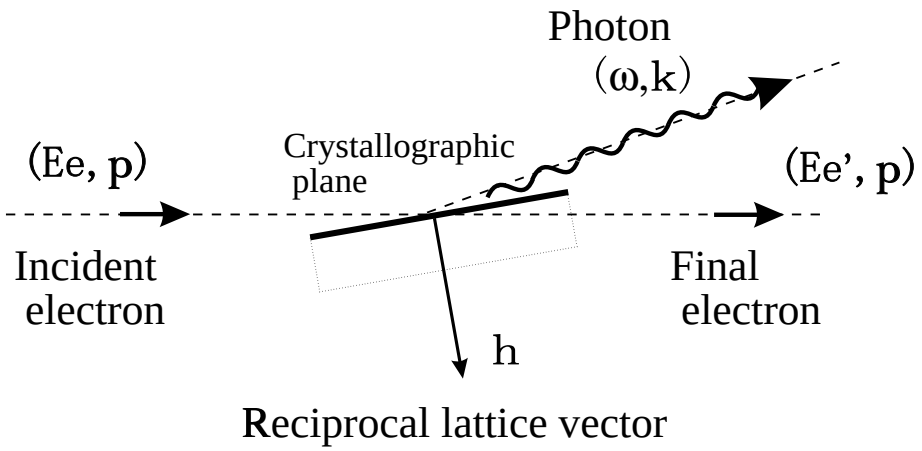

Figure 2: The relation of kinematical values.

$$\omega = \frac{\boldsymbol{v} \cdot \mathrm{h}}{1 - \boldsymbol{v} \cdot \mathrm{n}} \ , \tag{9}$$

where

$$\mathrm{n} \equiv \frac{\mathrm{k}}{|\mathrm{k}|} \ , \quad \boldsymbol{v} \equiv \frac{\mathrm{p}}{E_e} \ . \tag{10}$$

Likewise, the energy of Bragg reflection is

$$\omega_B = \frac{|\mathrm{h}|^2}{2\mathrm{h} \cdot \mathrm{n}_B} \ , \tag{11}$$

where

$$\mathrm{n}_B \equiv \frac{\mathrm{k}_B}{|\mathrm{k}_B|} \ , \tag{12}$$

ω_B and k_B are energy and momentum of Bragg reflected photon, respectively.

2.2.2 Differential Intensity

A model expressed by I.D.Feranchuk and A.V.Ivashin[2], called F-I model, is noted as a model of the differential intensity of PXR. By the recent works[5], it was found that the treatment of electron multiple scattering in their model was not in agreement with experimental results. The differential intensity[3, 4] by one electron passing through a unit length of the crystal is

$$\frac{d^2N}{d\Omega dz} = L \sum_h |\chi_{\mathbf{h}}|^2 \frac{\alpha\omega^3}{2\pi(1 - \boldsymbol{\beta} \cdot \mathbf{n})} \sum_\alpha \left| \frac{(\omega\boldsymbol{\beta} - \mathbf{h}) \cdot \mathbf{e}_{\mathbf{k}\alpha}}{(\mathbf{k} - \mathbf{h})_\perp^2 + (\omega/v)^2(1/\gamma^2 - \beta^2\chi_0)} \right|^2 \ , \tag{13}$$

where

$$v = |\boldsymbol{v}| \ , \quad \gamma = \frac{E_e}{m_e} \ , \quad \beta = |\boldsymbol{\beta}| = |\boldsymbol{v}|/c \ , \tag{14}$$

L is the thickness of the crystal, α is fine structure constant, χ_0 and $\chi_{\mathbf{h}}$ are the electric susceptibility and the Fourier components of the electric susceptibility for order 0 and $\mathbf{h}$, respectively. $\mathbf{e}_{\mathbf{k}\alpha}$ is the polarization vector of the scattered wave and c is the velocity of light. Intergrade the equation.(13) over the polarization of the emitted photon and assume $\omega \approx \omega_B$, and then

$$\frac{d^2N}{d\theta_x d\theta_y} = \frac{\alpha}{4\pi}\omega_B Z \frac{|\chi_{\mathbf{h}}|}{\sin^2\theta_B} \frac{\theta_x^2 \cos^2 2\theta_B + \theta_y^2}{(\theta_x^2 + \theta_y^2 + \theta_{ph}^2)^2} \ , \tag{15}$$

where

$$Z \equiv L_a[1 - \exp(-L/L_a)] \tag{16}$$

$$\omega_B \equiv \frac{\pi}{d \sin\theta_B} \ , \quad \theta_{ph}^2 \equiv 1/\gamma^2 + |\chi_0| \ , \tag{17}$$

θ_x and θ_y are the angular displacements away from the Bragg angle θ_B, and L_a is the absorption length of the crystal for x-rays of energy ω_B.

3 Measurements

Experiments were performed by using the 1.3GeV electron synchrotron at the Institute for Nuclear Study, University of Tokyo(INS). The electron energy was 1GeV(Fig.3.).

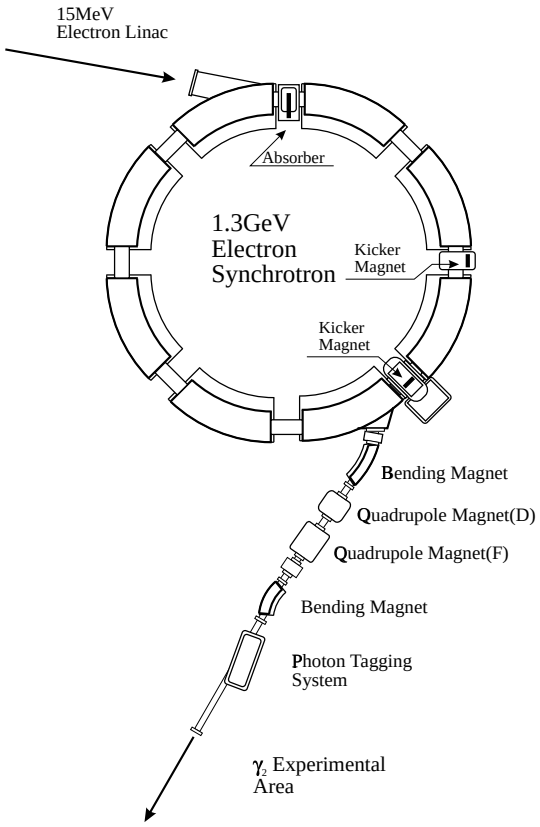

Figure 3: Layout of the γ_2-beam line at INS

3.1 Ordinary Method: using CCD camera

3.1.1 Experiments

3.1.1.1 Apparatus and Setup

The experimental set up is shown in Fig.4. The photon from a screen struck by the beam at a 45 degree angle, were detected by a CCD camera situated at right angle to the beam line. The distance from the camera(TM845 made by TAKENAKA SYSTEM.inc) to the fluorescent screen was 485mm. The image sensor size and the number of pixels of the CCD were $6.6mm(V) \times 8.8mm(H)$ and $487(V) \times 767(H)$,respectively. An active area

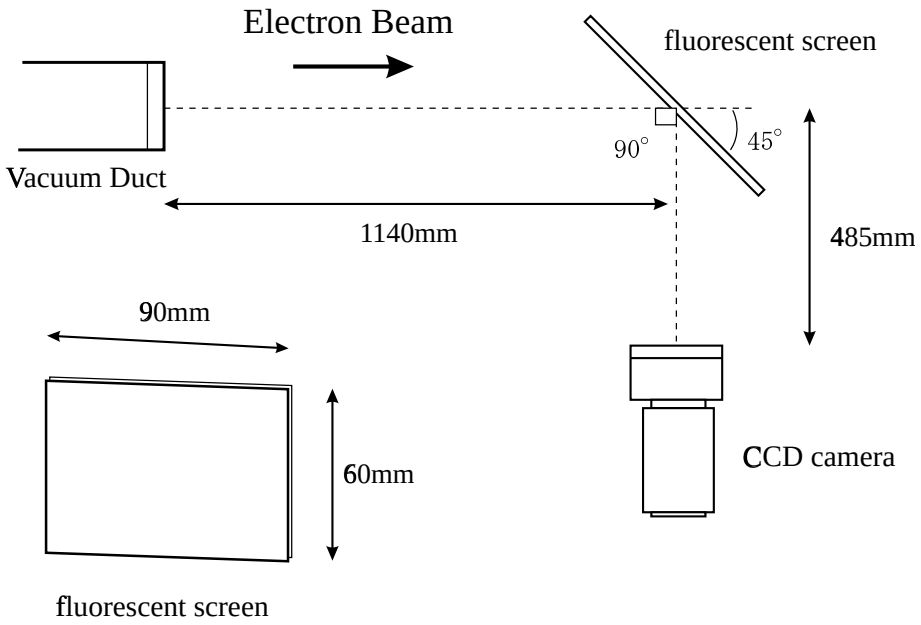

Figure 4: Setup

viewed by a camera was about $50(V) \times 70(H)mm^2$. The fluorescent screen painted ZnS was $60(V) \times 90(H)mm^2$.

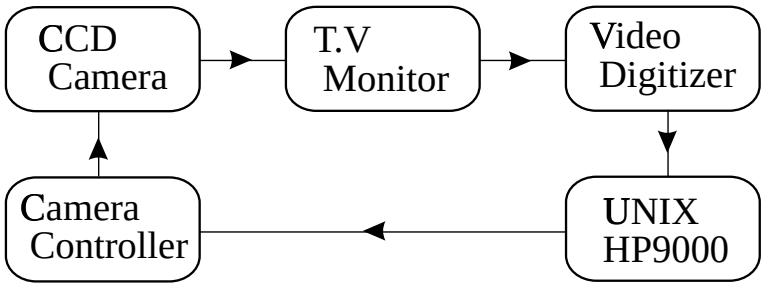

Figure 5: The relation of circuit modules

electronics The system of our electronics are shown in Fig.5. The analog-video signals of the camera were led to a video digitizer through a T.V monitor. The output signals were degitalized to 8 bit and transferred to a unix based workstation HP9000. A shutter speed of the CCD camera was controlled within the range 1/5000 to 1/125 (s). The shutter timing was controlled also by the workstation. The image data and the projection data for horizontal and vertical planes were stored in the hard disk of the

workstation.

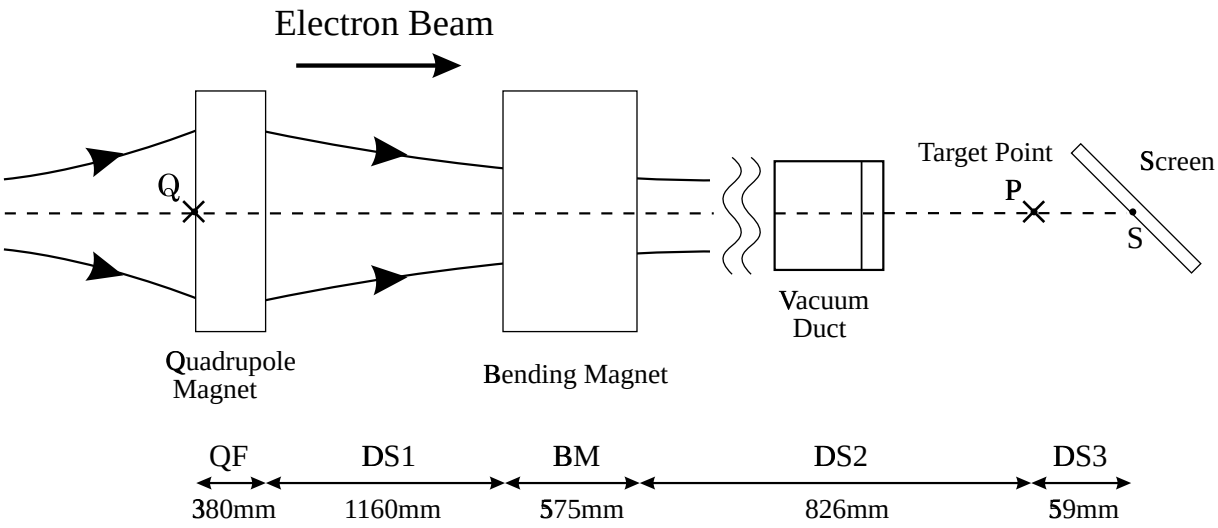

Figure 6: Optics of emittance measurement at the γ_2-Beam Line

3.1.1.2 Experimental Procedure The beam parameters were measured by the similar method as that used at SLAC[6]. The basic idea behind the method was to determine the beam size($\sqrt{\sigma_{11}}$) at a screen, with a profile monitor as function of the strength of an upstream quadrupole magnet(Fig.6.). We determined beam sizes with changing the quadrupole-magnet current at the range of 24.0 to 51.0 (A).

Theory of Measurements Write transfer matrices of drift spaces as M_{DS1}, M_{DS2} and M_{DS3}, and of a quadrupole magnet and a bending magnet as M_{QM} and M_{BM}, respectively, then the σ^Q matrix is propagated through the quadrupole and the drift space by the equation.(5) (p.3)

$$\sigma^S = R\sigma^Q R^T,$$

where σ^Q and σ^S are σ matrices at the entrance of the quadrupole(:position Q) and at the screen(:position S), respectively, and

$$R = M_{DS3}M_{DS2}M_{BM}M_{DS1}M_{QM}, \tag{18}$$

so,

$$\sigma_{11}^S = R_{11}^2\sigma_{11}^Q + 2R_{11}R_{12}\sigma_{12}^Q + R_{12}^2\sigma_{22}^Q. \tag{19}$$

The measured σ_{11}^S may be fit to a equation.(19), then the σ^Q is obtained. Emittance and Twiss parameters at the position Q, are calculated by the obtained σ^Q and the equation.(2)

$$\begin{aligned} \varepsilon &= \sqrt{\sigma_{11}^Q\sigma_{22}^Q - {\sigma_{12}^Q}^2} \\ \alpha &= -\sigma_{12}^Q/\varepsilon \\ \beta &= \sigma_{11}^Q/\varepsilon \\ \gamma &= \sigma_{22}^Q/\varepsilon. \end{aligned} \tag{20}$$

Therefore, Emittance and Twiss parameters downstream from the position Q, are calculated by equation.(6).

3.1.2 Data analysis

3.1.2.1 Beam Parameters The γ^2-beam line was as Fig.3. Fig.7 was integrated beam intensity in x(Horizontal) and y(Vertical) directions, respectively. The beam widths at the screen($\sqrt{\sigma_{11}^S}$) were acquired from a general gauss approximation to the measured data. Next, $(beam\ widths)^2$ were fit to equation.(19) (Fig.8), and from which, Emittance and Twiss parameters were obtained with equation.(20).

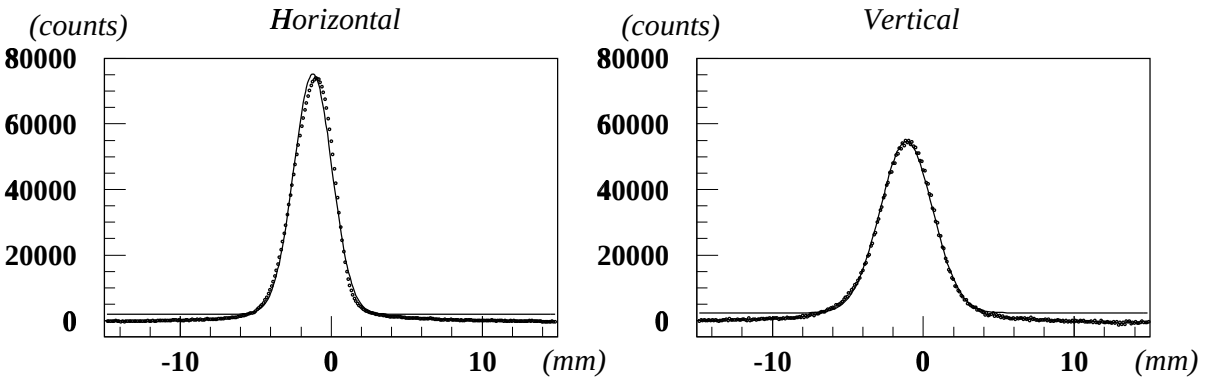

Figure 7: Spatial Distribution

Transfer-matrix equations.(25),(26),(27) and (29) were used, and parameters of the beam line elements used for the analysis of this section, were in Table.1.

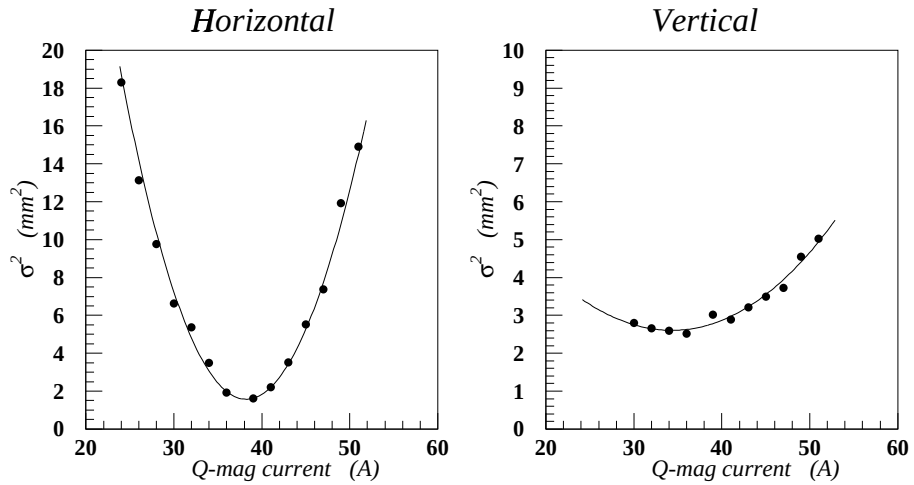

Figure 8: The square of beam width as a function of the quadrupole current.

Table 1: Parameters of the Beam Line Elements

Elements	*Length* [cm]	*Field* [kG/cm], [kG]	*Bending Angle* [mrad]
Quadrupole(QF)	38	0.87*	-
Drift space(DS1)	116	-	-
Bending (BM)	57.5	11.97**	172.0
Drift space(DS2)	826	-	-
Drift space(DS3)	59	-	-

*gradient of magnet field at 50[A]
**magnet field at 760[A]

3.1.2.2 Beam ellipse With emittance and twiss parameters obtained as described before, beam ellipses(1-σ) were given by equation.(1). In Fig.9, (a) and (b) were beam ellipses for horizontal and vertical planes at the entrance of the quadrupole magnet, respectively. Likewise, beam ellipses at the position P were obtained by parameters transfered with using equation.(6). Fig.9.(c) and (d) were ellipses calculated as the current of the quadrupole magnet were 45(A) for each planes, respectively.

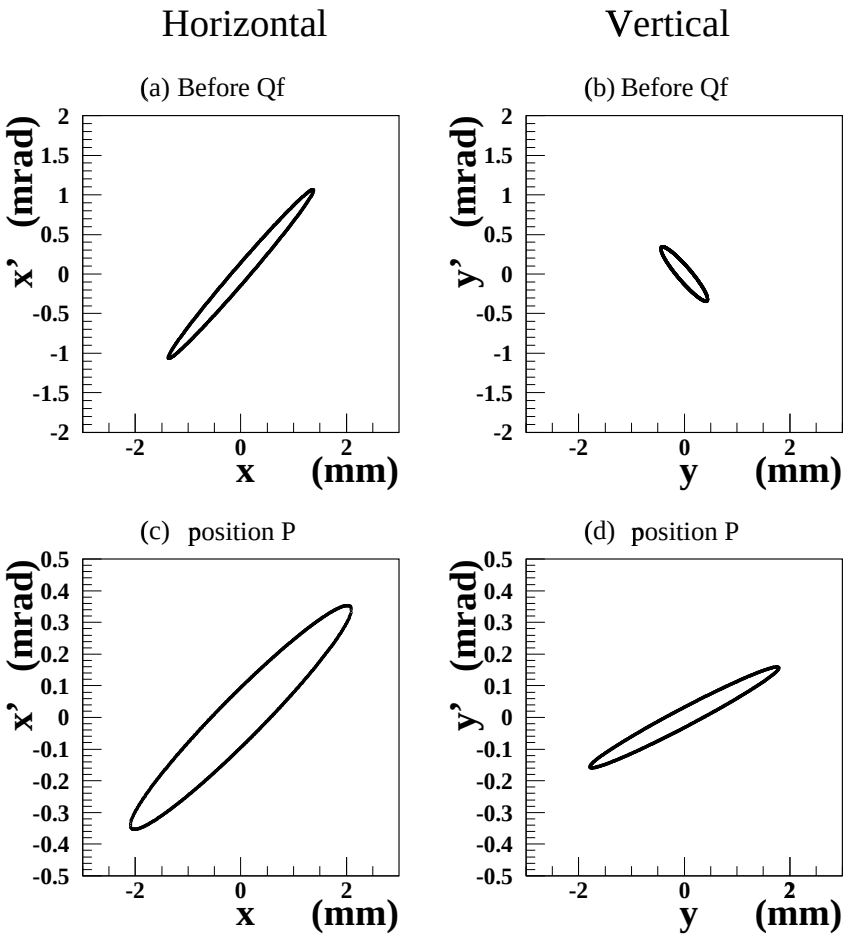

Figure 9: Beam Ellipse.

3.1.3 Results

As the result of analysis, the emittance, the twiss parameters, beam size(σ) and the tilt angle(χ) at the position Q and at the position P were obtained for horizontal and vertical planes, respectively. They are shown in Table.2 and in Table.3, The position Q and P

were a position of the entrance of a quadrupole magnet for focusing and the position of the Si target used in the PXR measurement, respectively(Fig.6). Beam size(σ) is 1-σ size of electron beam. In Table.3, 31(A), 38(A) and 45(A) are currents of the quadrupole magnet for under-focused, focused and over-focused beam, respectively.

Table 2: Emittance(ε), Twiss parameters, Beam size(σ) and Tilt Angle(χ) at Q.

Horizontal		**Vertical**	
ε_x (π·m·rad)	$1.98 \pm 0.03 \times 10^{-7}$	ε_y (π·m·rad)	$5.77 \pm 0.04 \times 10^{-8}$
α_x	-7.35 ± 0.11	α_y	2.44 ± 0.02
β_x	9.57 ± 0.15	β_y	3.41 ± 0.03
γ_x	5.75 ± 0.09	γ_y	2.04 ± 0.02
σ_x (m)	$1.38 \pm 0.0002 \times 10^{-3}$	σ_y (m)	$4.43 \pm 0.002 \times 10^{-4}$
χ_x (rad/m)	$6.58 \pm 0.001 \times 10^{-1}$	χ_y (rad/m)	$-6.50 \pm 0.004 \times 10^{-1}$

Table 3: Twiss parameters, Beam size(σ) and Tilt Angle(χ) at P.

Horizontal			
	31 (A)	38 (A)	45 (A)
α_x	-1.03 ± 0.02	$-5.68 \pm 0.24 \times 10^{-1}$	-3.59 ± 0.06
β_x	$2.86 \pm 0.05 \times 10$	7.21 ± 0.24	$2.21 \pm 0.04 \times 10$
γ_x	$7.18 \pm 0.23 \times 10^{-2}$	$1.83 \pm 0.37 \times 10^{-1}$	$6.29 \pm 0.10 \times 10^{-1}$
σ_x (m)	$2.38 \pm 0.008 \times 10^{-3}$	$1.20 \pm 0.02 \times 10^{-3}$	$2.09 \pm 0.01 \times 10^{-3}$
χ_x (rad/m)	$3.59 \pm 0.07 \times 10^{-2}$	$8.01 \pm 0.39 \times 10^{-2}$	$1.61 \pm 0.02 \times 10^{-1}$
Vertical			
	31 (A)	38 (A)	45 (A)
α_y	-4.25 ± 0.06	-3.94 ± 0.07	-4.85 ± 0.08
β_y	$4.15 \pm 0.06 \times 10$	$4.23 \pm 0.07 \times 10$	$5.57 \pm 0.09 \times 10$
γ_y	$4.58 \pm 0.06 \times 10^{-1}$	$3.90 \pm 0.06 \times 10^{-1}$	$4.41 \pm 0.07 \times 10^{-1}$
σ_y (m)	$1.55 \pm 0.01 \times 10^{-3}$	$1.56 \pm 0.01 \times 10^{-3}$	$1.79 \pm 0.01 \times 10^{-3}$
χ_y (rad/m)	$1.02 \pm 0.02 \times 10^{-1}$	$9.28 \pm 0.19 \times 10^{-2}$	$8.69 \pm 0.17 \times 10^{-2}$

3.2 New Method: using PXR

3.2.1 Experiments

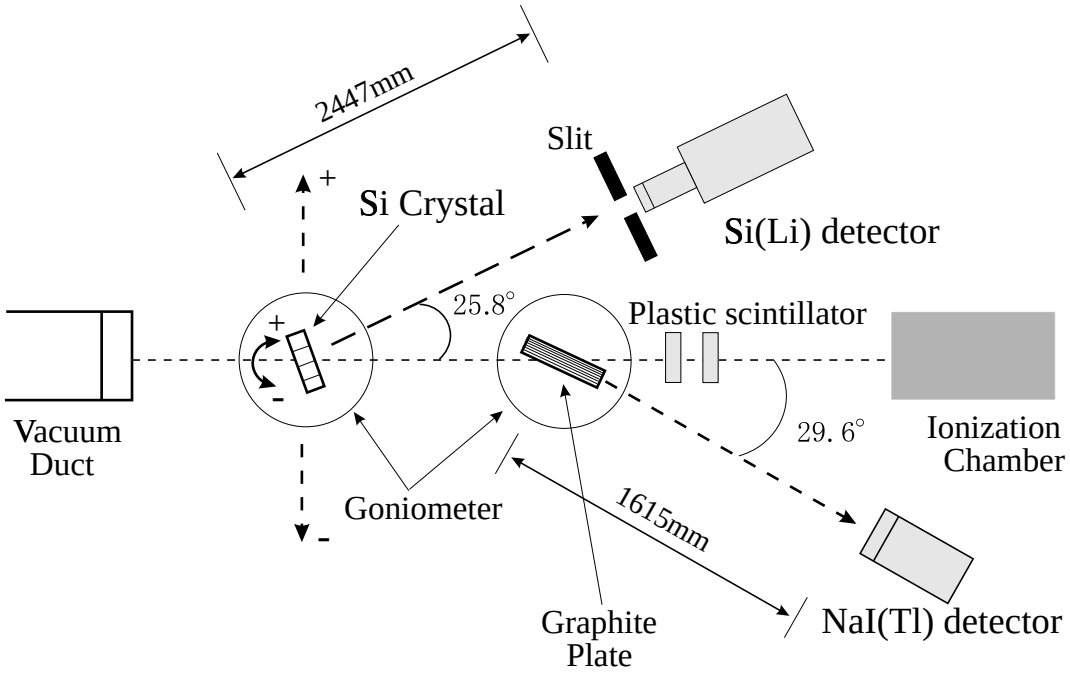

Figure 10: Setup

3.2.1.1 Apparatus and Setup The experimental set up is shown in Fig.10. The target crystal was a mono-crystalline silicon plate whose thickness was 0.5mm and area was $2 \times 2mm^2$. The surface of the plate was parallel to the (112) crystallographic plane. The target mounted on a computer-controlled three-axis goniometer in air. The resolution of the goniometer around the y axis is about 0.07mrad. A Si(Li) photon detector was used for detecting PXR. The detection angle and the energy of PXR were about 25.8° and 14.4keV,respectively. The Si(Li) detector was set on a computer-controlled table movable in the horizontal plane perpendicular to the x-ray emission angle,at 2447mm away from the crystal. The resolution of the table is 2μm. The diameter of Si(Li) was 16mm and the thickness was 5.7mm. A vertical slit with a 10mm opening was placed in front of the detector. The energy resolution of the detector at 14.4keV is 3.6%. In order to measure the absolute intensity, a graphite plate,plastic scintillators and an ionization chamber were set at 845mm,1492mm and about 6000mm downstream from the silicon target,respectively. The graphite plate, mounted on a computer-controlled two axis goniometer in air, was

$30 \times 30mm^2$ and the thickness was 2mm. The surface of the plate was parallel to the (002) crystallographic plane. To detect the PXR from the graphite, a NaI(Tl) detector was equipped at 1615mm from the graphite. The detection angle was about 29.6° at 14.4keV.

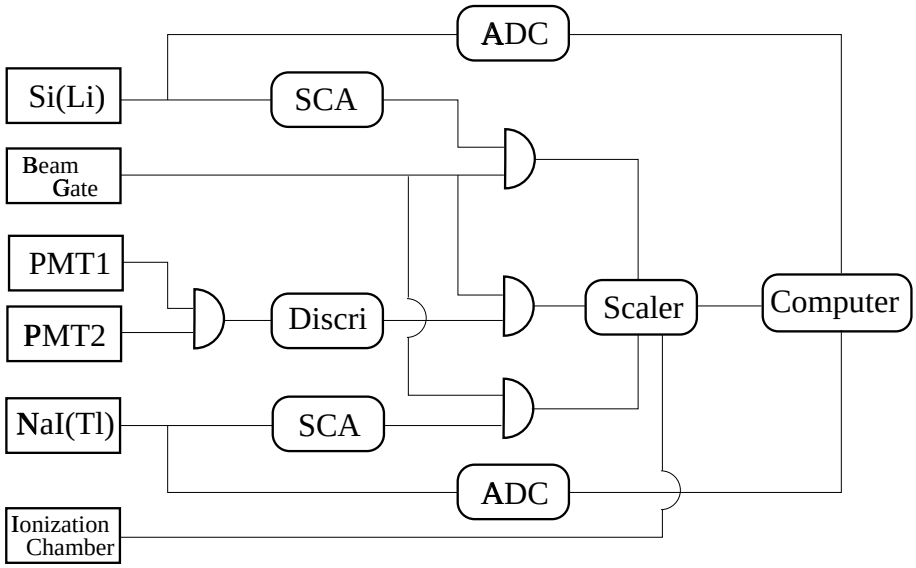

Figure 11: The relation of circuit modules

electronics The system of our electronics are shown in Fig.11. The signals from Si(Li) detector and NaI(Tl) detector were led in a Single Channel Analyzer(SCA) and an Analog-Digital Converter(ADC) after being amplified,respectively. SCA can discriminate the input pulse height being in the range between the two discrimination levels,and outputs logic pulse. These pulse and the pulse from Ionization chamber were counted by a CAMAC standard scaler. The ADC is used for analyzing the pulse hight. The coincidental signals from plastic scintillators were led in a discriminator of which output signals were also counted by CAMAC scalar. All of these signals were transferred to the personal computer. The goniometers for the silicon crystal and the graphite, and the movable table for Si(Li) detector were remotecontorolled by the same computer.

3.2.1.2 Experimental Procedure

absolute intensity As beam intensity is not stable while a measurement, it is necessary to obtain the correct value of an absolute intensity of PXR for electrons. In order to count a number of electrons, plastic-scintillation counters were used. But there was no region of electron-beam intensity where both the dead time of scintillators and the background counted by a Si(Li) detector to detect x rays from the silicon target, were ignored. At the beam intensity where the Si(Li) detector was usable, an ionization chamber to detect a relative number of electrons was usable. While at the beam intensity① where the scintillators were usable, a NaI(Tl) scintillation counter to detect x rays from the graphite was usable, as PXR form the graphite was higher intensity than from the silicon target. To obtain an absolute number of electrons by using the ionization chamber, following method was took. First, at intensity①, a counting ratio①: NaI(Tl)/PMT was obtained, where 'PMT ' was coincidental counts of two plastic scintillators. Second, at the intensity where the NaI(Tl) and the Ionization Chamber were usable, a counting ratio②: (Ionization Chamber)/NaI(Tl) was obtained. Accordingly, absolute intensity of the PXR from Si target was measured by a counting ratio of the Si(Li) detector and the Ionization Chamber ;

$$\frac{PXR}{electron} = \frac{Si(Li)}{Ionization\ Chamber} \times (counting\ ratio①) \times (counting\ ratio②) \qquad (21)$$

Ratios of ① and ② were obtained by Fig.12.(a), (b) and the beam intensity for the experiment was determined by Fig.12.(c), where ratio①, ② and ③ were plotted with changing beam intensity, respectively.

Measurement of the beam distribution The intensity of PXR was measured with changing the rotation angle, tilt angle, horizontal and vertical position of the target crystal to find the center of the electron beam. At the center of the electron beam(position 1 in Fig.13.), the rocking curve and spectrum of PXR were measured. Next, the horizontal position of the target and the detector were moved by 2.0mm(position 2). The rocking curve was acquired and the spectrum was measured at an angle of the target fixed to the peak angle of rocking curve. The above measurements were repeated with the horizontal position of both the target and the detector changed by 2mm step at same

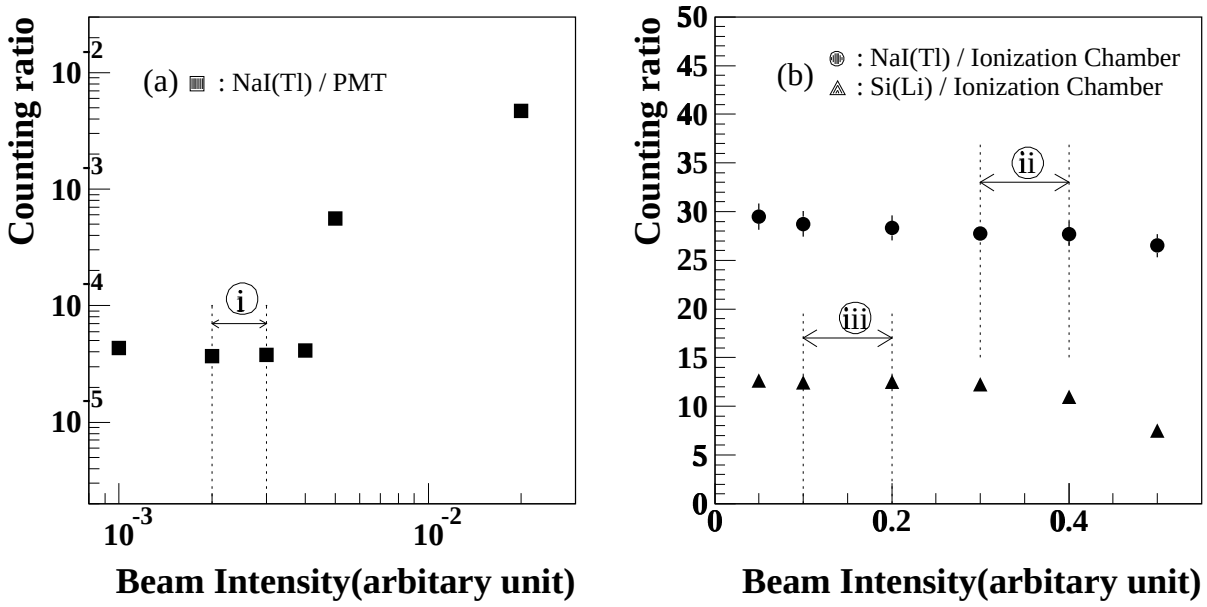

Figure 12: Counting ratios for beam intensities.

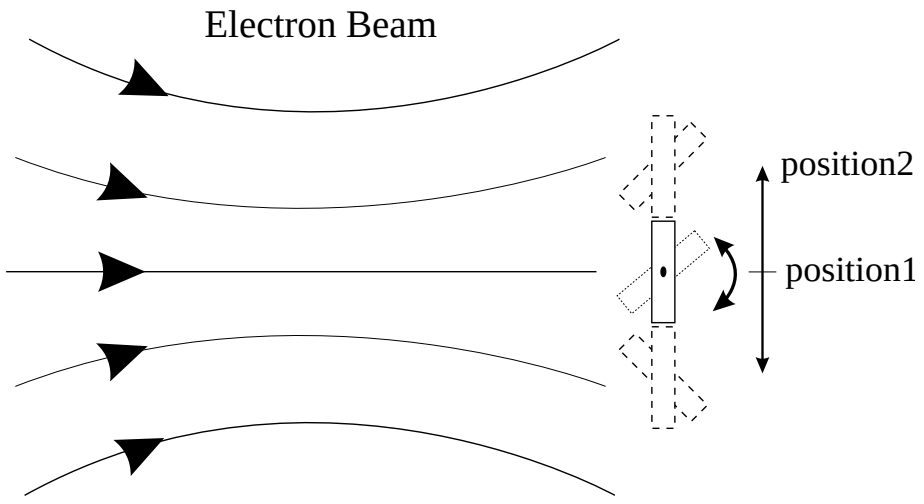

Figure 13: Measurement of the beam distribution

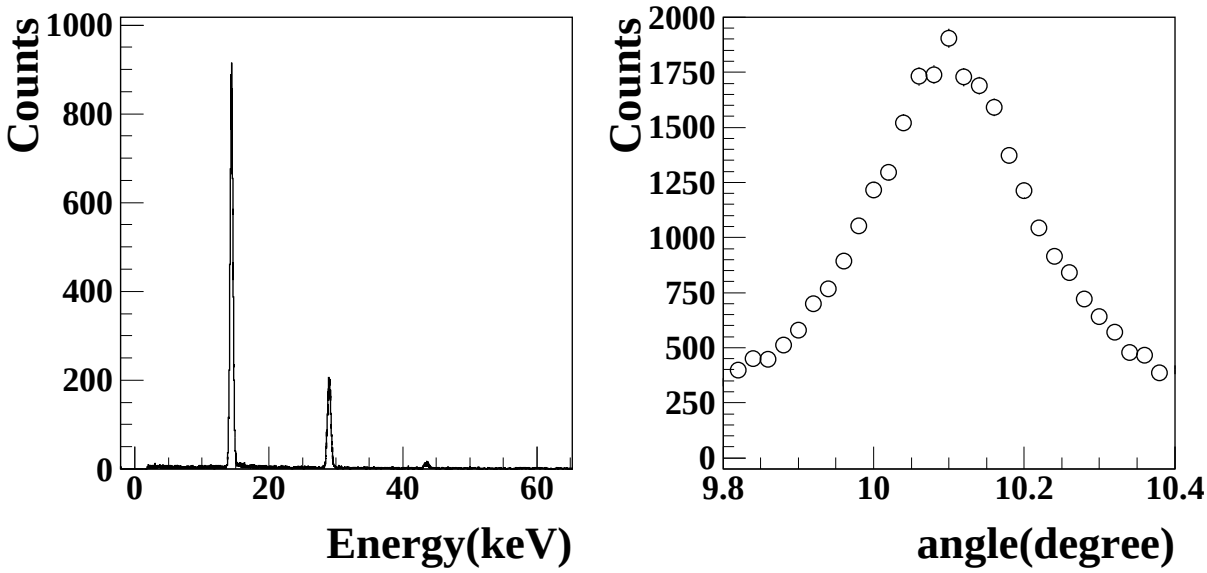

Figure 14: The energy spectrum and the rocking curve of PXR.

time, under conditions of over-focused and under-focused beams, respectively. A typical energy spectrum and rocking curve of PXR, are shown in Fig.14.

3.2.2 Data analysis

3.2.2.1 absolute intensity At the intensity where two detectors are usable, it is found that counting ratio of detectors should be constant. And then from Fig.12, ratio ①, ② and ③* were obtained in Table.4. Where counts of Si(Li) detector were measured by using the Si target which of thickness was 0.5mm and of area was enough larger than focused beam size, and ratio③* was acquired by ratio① and ② (from equation.(21)).

Table 4: absolute intensity.

		counting ratio
①	NaI(Tl)/PMT	$3.71 \pm 0.17 \times 10^{-5}$
②	(Ionization Chamber)/NaI(Tl)	$3.61 \pm 0.16 \times 10^{-2}$
③	Si(Li)/(Ionization Chamber)	$1.22 \pm 0.29 \times 10$
③*	PXR/e^-	$^{*}1.63 \pm 0.40 \times 10^{-5}$
		$^{**}8.63 \pm 2.13 \times 10^{-6}$

*ratio of PXR, at full spectrum, for a electron.
**ratio of PXR, at 14.4keV, for a electron.

3.2.2.2 Beam distribution Rocking curves obtained by measurements were fit to equation.(22), where θ is angle of the target crystal and M, θ_a, θ_W, a, b and c are parameters determined by fit. And then PXR intensities for each crystal position were acquired as peak counts of rocking curves. The parameter 'a' determined by fit is the peak angle of rocking curve. Fig.15.(a) shows PXR intensities(arbitrary unit) for five position, where Qf current was 45(A) (over-focused beam). Accordingly, convert absolute PXR intensities to beam intensities by ③* (in Table.4), and then beam sizes were obtained by fitting the beam distribution (or Fig.15.(a)) assumed a general Gaussian distribution.

$$N(\theta) = M\frac{\theta_a^2(\frac{\theta-a}{2})^2+\theta_W^4}{\{(\frac{\theta-a}{2})^2+\theta_W^2\}^2} + b(\theta-a)+c \tag{22}$$

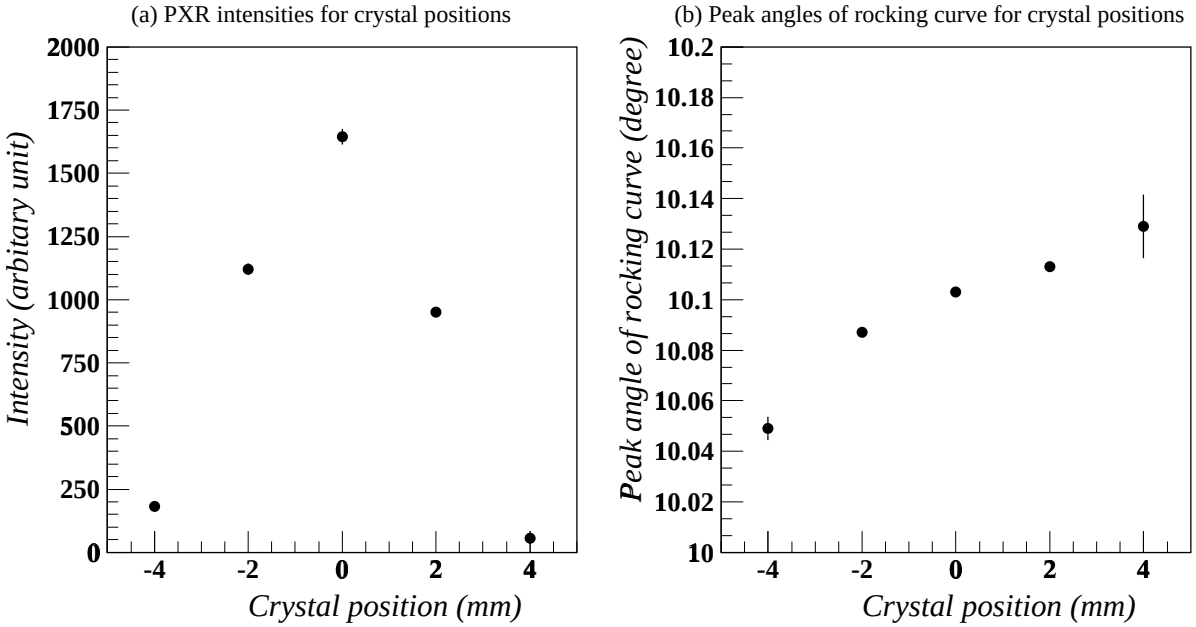

Figure 15: Beam distribution

3.2.2.3 Beam divergence Fig.15.(b) shows the distribution of peak angles of rocking curves for each crystal position, Qf current was 45(A) as before. The parameter χ, the tilt angle of ellipse in phase space, was acquired by liner fit to the distribution.

3.2.3 Results

As the result of analysis, beam sizes(σ_x) and tilt angles(χ_x) of ellipse in phase space at horizontal plane were obtained for under-focused and over-focused beams, respectively. They are shown in Table.5, where 31(A) and 45(A) are currents of a quadrupole magnet for focusing, and σ_x is 1-σ size of electron beam.

Table 5: Beam size and Tilt Angle of the ellipse in phase space.

	31 (A)	45 (A)
σ_x (m)	$2.15 \pm 0.25 \times 10^{-3}$	$2.27 \pm 0.10 \times 10^{-3}$
χ_x (rad/m)	$7.2 \pm 1.8 \times 10^{-2}$	$2.05 \pm 0.12 \times 10^{-1}$

4 Discussion

Tilt angle(χ)s of ellipse in phase space, obtained by new method(PXR) and ordinary method(CCD), are about 0.21[rad/m] and 0.16[rad/m] at 45[A], respectively. Fig.16 shows peak angles of beam divergence, obtained by the PXR and by the CCD, for five crystal positions(or regions), where black circles are peak angles by the PXR mesurement and white circles are peak angles(integrated for 2mm width) by the CCD mesurment for crystal positions. The dotted line and solid line are the liner fit of five white circles and of three black circles(at $-2, 0, 2$mm), respectively. And the peak angle of beam divergence was nomalized zero at positon zero. From these fit, χ for two mesurements(by the PXR and the CCD) are 0.16[rad/m] and 0.15[rad/m], respectively, and they are well in agreement. While the peak angle for other crystal positions are not in agreement. And some spatial distributions mesured by the CCD are Two Gaussian distributions rather than the general gaussian distributions. This means that beam ellipse may become like as Fig.17 if a spatial distribution is separated into two beam distributions by fitting it with Two Gaussian. It was, therefore, possibility that the peak angle of anglular divergences was like as Fig.16 in the part out of about 1-σ.

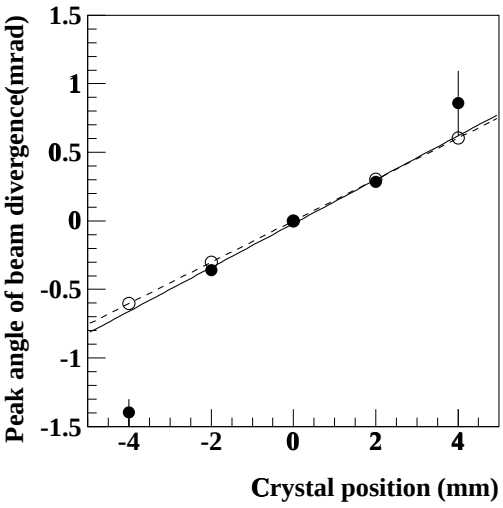

Figure 16: Beam Divergence for Crystal position

Next, in order to estimate the beam anlgur distribution, Monte Calro simulation for the PXR was performed by using equation.(15). Fig.18 shows the Monte Carlo simulation for the rocking curve. Measured data of the rocking curve are plotted with black circles.

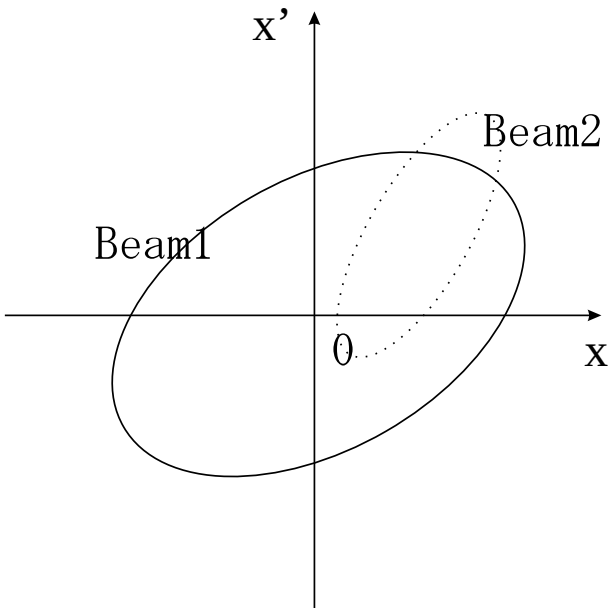

Figure 17: Beam Distribution in phase space in the case of Two Gauss.

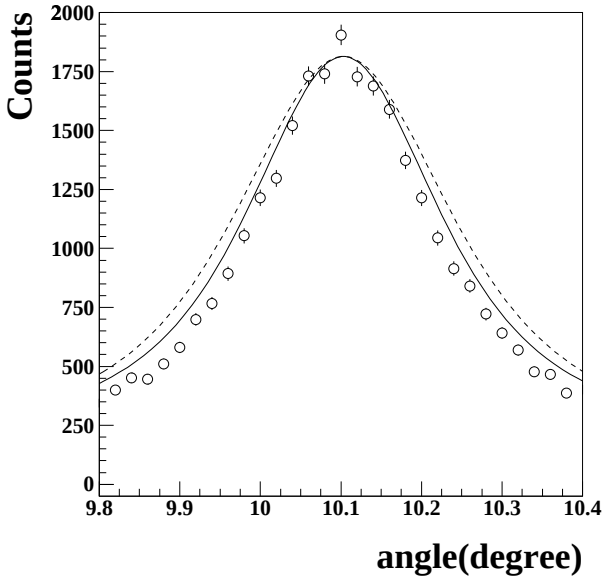

Figure 18: Monte Carlo simulation of PXR

The white circles and triangles are output data obtained by the simulation assuming the beam divergence(FWHM) $\delta\theta = 0$[mrad] and $\delta\theta = 7$[mrad], respectively. It is found that the width of the experimental data is narrower than the simulation even for $\delta\theta = 0$. This means that the theoretical formula involved in the simulation under-estimate the beam divergence.

5 Conclusion

We have proposed a new method of beam diagnostics based on the characteristic features of parametric x radiation and estimated its feasibility. In the test experiment we found that the spatial-angular correlation of the beam was consistently measured by the new method. In order to gain further information for the electron distribution in the beam ellipse by this method, it is necessary to use smaller crystal and to refine theoretical treatment of the parametric x radiation.

6 Acknowledgments

The author would like to express his gratitude to Professor I. Endo for his guidance. The author also would like to thank Professor Horiguchi, Dr. Takahashi, Mr. Y. Takashima to support the author. This experiments would have been impossible without the help of the operation crew of Electron synchrotron at the Institute for Nuclear Study, University of Tokyo. The author is grateful to Professor K. Yoshida, Dr. M. Muto, Mr. Y. Hashimoto for their collaboration and give many useful advices.

References

[1] M.L. Ter-Mikaelian, *High-Energy Electromagmetic Process in Condensed Media* (Wiley-Interscience, New York, 1972).

[2] I.D. Feranchuk and A.V. Ivashin, J.Phys.(Paris) **46**, 1981 (1985).

[3] H. Nitta, Phys.Lett.A **158**, 270 (1991).

[4] H. Nitta, Phys.Rev.B **45**, 7621 (1992).

[5] S. Asano, I. Endo et al., Phys.Rev.Lett **70**, 3247 (1993).

[6] M.C. Ross, N. Phinney, G. Quickfall, H. Shoaee, J.C. Sheppard, **SLAC-PUB-4278** (1987).

[7] C. Bovet and et al.,
A Selection of Formulae and Data useful for the Design of A.G. Synchrotroms, CERN/MPS-SI/Int. DL/70/4

[8] M. Castellano, M. Ferrario et al., Nucl. Instr. and Meth. **A 357** (1995) 231

[9] Y. Hashimoto, M. muto et al., **INS-T-511**, (1992)

A Transfar Matrix

A ring or beam line is composed of drift space, bending magnet ,quadrupole magnet and so on. A bending magnet and a quadrupole magnet are used to bend a particle and to focus(or defocus) a particle, respectively. In a ring(or beam line), a particle follows orbit theory. The first order equation of transverse(x) motion of a particle along the beam line(s axis) is written as

$$\frac{d^2x}{ds^2} + K(s)x = 0 \ . \tag{23}$$

Write the position and angle of the particle trajectry as a vector (x, x') and define that there is nothing($K(s) = 0$) between point 1 and point 2 along the beam line and that the length between them is L(, called as drift space), and then following equation is obtained by equation(23),

$$\begin{pmatrix} x \\ x' \end{pmatrix}_2 = \begin{pmatrix} 1 & L \\ 0 & 1 \end{pmatrix} \begin{pmatrix} x \\ x' \end{pmatrix}_1 \qquad (x' \equiv \frac{d^2x}{ds^2}) \ , \tag{24}$$

and then a matrix(,called as 'Transfar Matrix',) of drift space(M_{drift}) is written as,

$$M_{drift} = \begin{pmatrix} 1 & L \\ 0 & 1 \end{pmatrix} \ . \tag{25}$$

Likewise, define $K(s) \equiv K(= const \neq 0)$, and then transfar matrices(M_{QF} and M_{QD}) of quadrupole magnets for focusing and defocusing are obtained, respectively.

If $K > 0$,

$$M_{QF} = \begin{pmatrix} \cos\sqrt{K}L & \frac{1}{\sqrt{K}}\sin\sqrt{K}L \\ -\sqrt{K}\sin\sqrt{K}L & \cos\sqrt{K}L \end{pmatrix} \ , \tag{26}$$

if $K < 0$,

$$M_{QD} = \begin{pmatrix} \cosh\sqrt{|K|}L & \frac{1}{\sqrt{|K|}}\sinh\sqrt{|K|}L \\ \sqrt{|K|}\sinh\sqrt{|K|}L & \cosh\sqrt{|K|}L \end{pmatrix} \tag{27}$$

, where L is the length of quadrupole magnet along the beam line and K , called as Kvalue[m^{-2}], is defined as

$$K \equiv \frac{1}{p}\frac{\partial B}{\partial x}\ ,\ \frac{1}{p}\frac{\partial B}{\partial y} \qquad (\frac{\partial B}{\partial y} = -\frac{\partial B}{\partial x}) \tag{28}$$

, where p is momentum of a particle[GeV/c]. $\partial B/\partial x$ and $\partial B/\partial y$ are gradients[T/m] of quadrupole field in horizonal plane and in vertical plane, respectively.

If a particle is bended in horizontal plane, matrices(M^H_{BM} and M^V_{BM}) of a bending magnet, for horizontal and vertical planes, is written as

$$M^H_{BM} = \begin{pmatrix} \cos\theta & \rho\sin\theta \\ -\frac{\sin\theta}{\rho} & \cos\theta \end{pmatrix}, \quad M^V_{BM} = \begin{pmatrix} 1 & \rho\theta \\ 0 & 1 \end{pmatrix} \tag{29}$$

,where θ and ρ are a bending angle and a radias of the curvature, respectively. These matrices is obtained by the equation(23) defined $K(s) \equiv 1/\rho^2 (M^H_{BM})$ and $K(s) \equiv 0 (M^V_{BM})$.